Applied Surface Science 598 (2022) 153792

Contents lists available at ScienceDirect

Applied Surface Science

journal homepage: www.elsevier.com/locate/apsusc

Full Length Article

Accessibility of grafted functional groups limits reactivity of covalent graphene derivatives

Martin Pykal [a,1], Martin Vondrák [a,1], Martin Šrejber [a], Iosif Tantis [a], Elmira Mohammadi [a], Aristides Bakandritsos [a,c], Miroslav Medveď [a], Michal Otyepka [a,b,*]

[a] Regional Center of Advanced Technologies and Materials, The Czech Advanced Technology and Research Institute (CATRIN), Palacký University Olomouc, Šlechtitelů 27, 779 00 Olomouc, Czech Republic

[b] IT4Innovations, VŠB – Technical University of Ostrava, 17. listopadu 2172/15, 708 00 Ostrava-Poruba, Czech Republic

[c] Nanotechnology Centre, Centre of Energy and Environmental Technologies, VŠB–Technical University of Ostrava, 17. listopadu 2172/15, 708 00 Ostrava-Poruba, Czech Republic

ARTICLE INFO

Keywords:
Accessibility
Reactivity
Reduction
Nitrile
Cyanographene
Molecular dynamics

ABSTRACT

Graphene derivatives are an emerging and important class of promising materials because they can bear a wide variety of functional groups, rendering them suitable for a plethora of applications, ranging from energy storage to sensorics. Further functionalisation of these materials requires a thorough understanding of their reactivity at the molecular level because the organic functional groups are close to an effectively infinite surface, which may affect their reactivity. Nitrile groups grafted on a graphene can be easily hydrolysed to carboxyl groups, but they are resistant to reduction by $LiAlH_4$. Here, we combine theoretical and experimental methods to explain the resistance of CN groups grafted on the graphene surface in terms of the limited accessibility of these groups for the reduction agent. We highlight that such mechanistic aspects, i.e., steric hindrance of the reaction centres and surface-solvent interactions, play a crucial role in the reactivity of 2D materials.

1. Introduction

Due to its unique physical–chemical properties, graphene[1] has attracted increasing attention from scientists across a wide spectrum of research fields.[2–5] Its rich chemistry, expanded via either noncovalent or covalent functionalisation routes, significantly extends the range of possible graphene applications, such as water decontamination[6,7], biomedicine [8,9], optics [10,11], composites[12,13] and electronic devices[14–16]. Covalent graphene functionalisation is particularly attractive because it enables band gap modulation, magnetism imprinting and control over hydrophilicity.[17–19] However, direct covalent graphene functionalisation is hampered by its chemical inertness, which can be overcome by defects, mechanical stress or harsh reaction conditions, such as application of plasma, strong oxidizing agents or radicals.[20–23,57] Fluorinated graphene, i.e. fluorographene (FG), enables a variety of novel synthetic routes in graphene derivatisation.[24] This well-defined stoichiometric graphene derivative behaves as an electrophile, and its reactions with nucleophiles lead to alkyl, aryl and nitrile derivates.[24,25] Reaction of FG with cyanides is particularly attractive because it establishes out-of-plane C–C bonds perpendicular with respect to the graphene lattice, and the grafted nitrile group permits further chemical modifications.[26–28] In particular, reaction of FG with NaCN in dimethylformamide (DMF) leads to cyanographene (GCN) with a nitrile functionalisation degree as large as ~15 %.[28] In molecular organic synthesis, nitriles are versatile precursors for the preparation of amines, amides, aldehydes, carboxylic acids, ketones and various heterocyclic compounds.[29–33] The nitrile functionalities of GCN have been successfully transformed to carboxyl groups (forming graphene acid, GA) by acidic hydrolysis of GCN with 20% HNO_3. On the other hand, reduction of GCN to graphene-amine does not seem to be easily achievable.

The abovementioned reactions of GCN are associated with the reactivity of the carbon–nitrogen triple bond. In acid-catalysed nitrile hydrolysis, the first reaction step involving protonation of the C≡N group facilitates the subsequent nucleophilic attack of water. The formed amide can then be converted to a carboxylic acid under

Abbreviations: FG, fluorographene; GCN, cyanographene.

* Corresponding author.
E-mail address: michal.otyepka@upol.cz (M. Otyepka).

[1] These authors contributed equally.

https://doi.org/10.1016/j.apsusc.2022.153792
Received 8 April 2022; Received in revised form 12 May 2022; Accepted 23 May 2022
Available online 26 May 2022

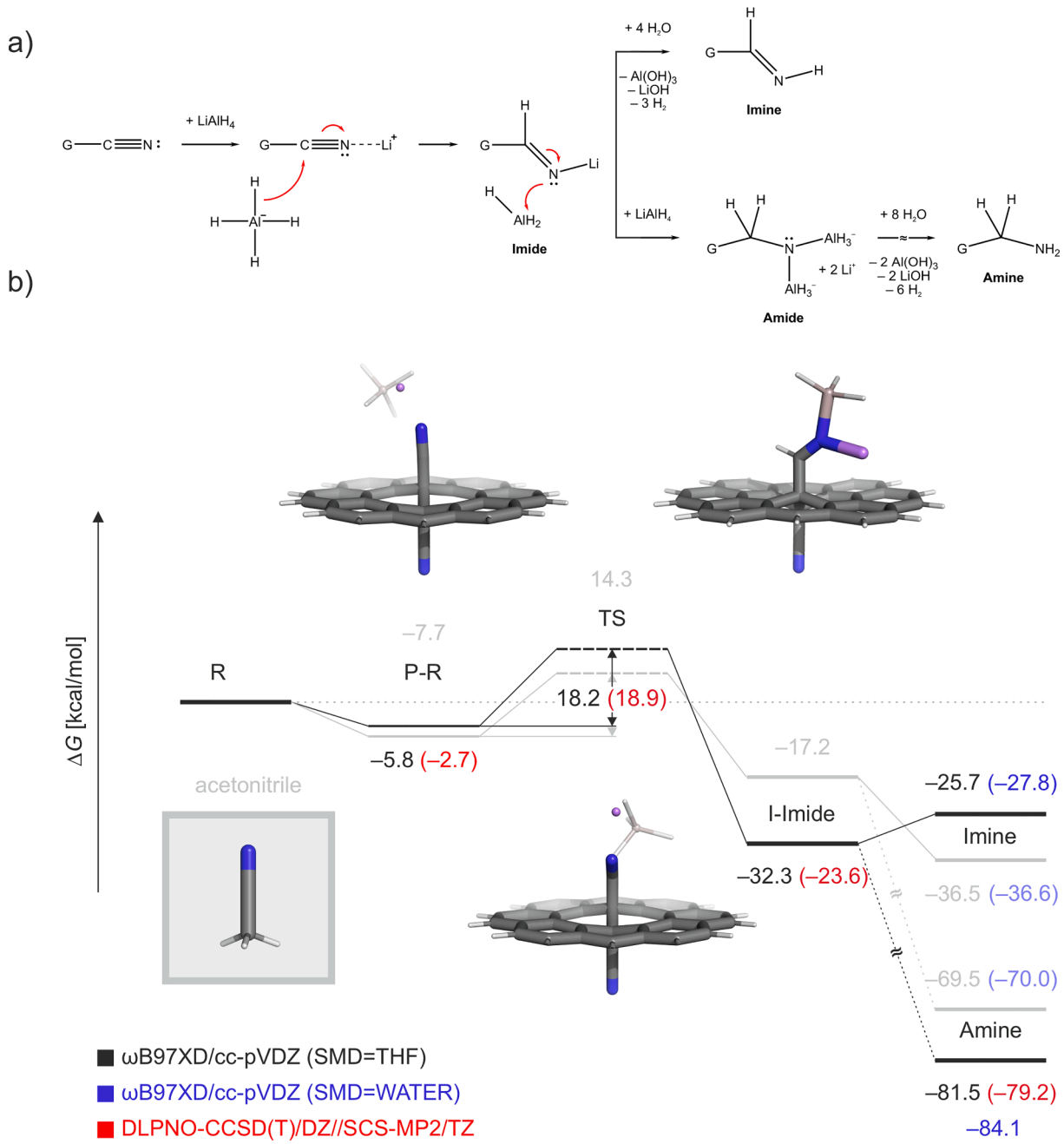

Fig. 1. a) Scheme for the suggested mechanism of the reduction of GCN, and b) reaction Gibbs energy (T = 298.15 K) profile for the reduction of GCN (acetonitrile in grey) by $LiAlH_4$. All values are in kcal/mol and were calculated at ωB97XD/cc-pVDZ level of theory (SMD = THF). The blue values in parentheses show the energetic balance when the last step was run in water (SMD = water). ΔG values calculated using high-level ab-initio composite approach DLPNO-CCSD(T)/DZ//SCS-MP2/TZ (on ωB97XD/cc-pVDZ level optimised geometries) are given in red. Colouring scheme: grey, carbon; purple, lithium; pink, aluminium; blue, nitrogen; white, hydrogen.

conditions of additional heat and excess of reactants. On the other hand, molecular nitriles can be reduced to primary amines using strong reducing agents, e.g. $LiAlH_4$. According to a generally accepted mechanism (Fig. 1a), the hydride anion AlH_4^- attacks the electron-deficient nitrile carbon, followed by electron transfer to nitrogen, leading to an imide intermediate that can then be either transformed to an imine or further reduced to an amine in the aqueous environment.[34,35] Previous density functional theory (DFT) calculations of formaldehyde reduction by $LiAlH_4$ have revealed a general configuration of the reactant state for the reduction of the carbonyl group in tetrahydrofuran (THF)[36] that may also be applicable for other functional groups following a similar mechanism and conditions. Thus, to initiate the reduction reaction, $LiAlH_4$ needs to be aligned with the carbonyl group in one plane with the torsional angle between C, O/N heteroatom, Li^+ and aluminium close to zero. In graphene chemistry, $LiAlH_4$ based reductions of various graphene derivatives, including graphene oxide, graphene azide and fluorographene, have been reported.[37–40] However, in GCN, despite the conversion of the –CN group to –COOH has been shown to be successful,[28] its conversion to an amine was not possible (see below and SI for experimental details). This surprising observation deserves further attention, especially considering the achievable reduction of other graphene derivatives by $LiAlH_4$.[37].

In the present study, we employed quantum mechanical (QM) methods and classical molecular dynamics (MD) simulations to study

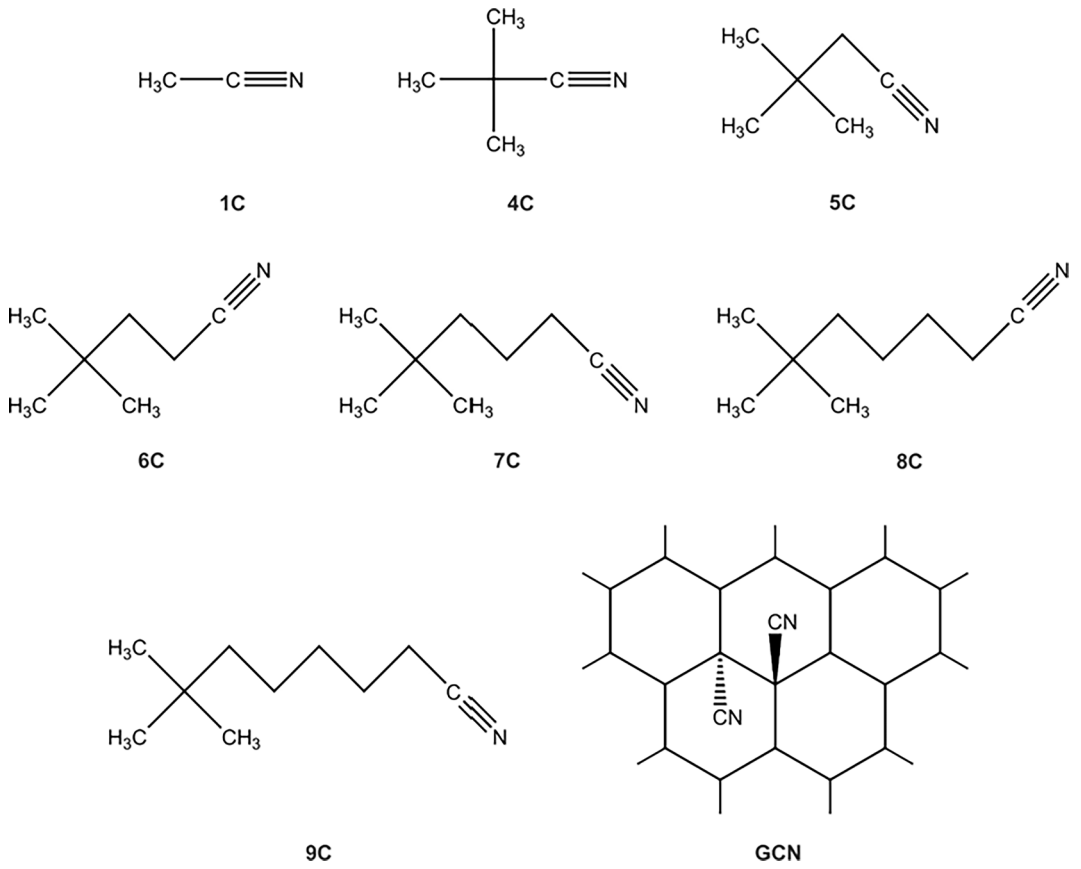

Fig. 2. Considered structures of nitriles differing in aliphatic chain length. The numbering is derived from an alkyl created by cleavage of the bond between carbon and the CN group, with the only exception of a 4C nitrile group that is attached to tertial carbon.

the thermodynamic, kinetic, and sterical aspects of GCN reduction by $LiAlH_4$ reducing agent in THF. In particular, the reaction profile of the reduction reaction and accessibility of $LiAlH_4$ to nitrile groups of GCN were examined. The acquired data were compared with those calculated for several representative aliphatic nitriles. The results indicated that there was limited accessibility of the reducing agent to the nitrile carbon atom due to its direct bonding to the graphene sheet acting as a steric barrier, which may explain the poor reduction of cyanographene's –CN groups to amines. This was consistent with solid-state NMR and FTIR measurements confirming the resistance of GCN towards $LiAlH_4$. Our findings show that the already rich chemistry of graphene may present further, previously elusive, inspiring aspects, whereby graphene may play the role of a selective sterically protecting group, as in the case of the chemistry of nitriles, allowing their transformation to carboxylic groups but not to amines. These findings could find applicability in complex reactions to synthesise products in a selective way, which under normal conditions would not be viable.

2. Methods

Fourier-transform infrared spectroscopy (FT-IR) was performed on an iS5 FTIR spectrometer (Thermo Nicolet) using the Smart Orbit ZnSe attenuated total reflection (ATR) accessory. Briefly, a droplet of the dispersed material was placed on the ZnSe crystal and left to dry. The spectra were acquired under a nitrogen gas flow through the ATR accessory.

X-ray photoelectron spectroscopy (XPS) was performed with a PHI VersaProbe II (Physical Electronics) spectrometer using an Al Ka source (15 kV, 50 W). The obtained data were evaluated with the MultiPak (Ulvac – PHI, Inc.) software package.

The solid-state NMR measurements were performed using a JEOL spectrometer JNM-ECZ400R with a superconducting coil having a magnetic field of 9.4 T (working frequency: 399.8 MHz for ^{1}H, and 100.5 MHz for ^{13}C) equipped with a 3.2 mm MAS probe. The ^{1}H–^{13}C cross-polarization magic angle spinning (CP-MAS) NMR spectra were collected at ambient temperature at the spinning rate of 18 kHz, using contact time and relaxation delay 8 ms and 6 ms, respectively, for all measurements.

At the QM level, GCN was modelled as a large polycyclic aromatic hydrocarbon (PAH) molecule, ovalene ($C_{34}H_{14}$), with single –CN functionalisation on each side. In DFT calculations, the ωB97XD functional [41] with the cc-pVDZ basis set[42] with superfine grid settings using the spin-unrestricted formalism was employed for geometry optimisation and vibrational frequency calculations. For optimised structures, single point energy calculations were performed using the cc-pVTZ basis set.[42] The implicit solvation model based on density (SMD)[43] was used to account for the effects of the solvent (THF) environment. Transition state (TS) structures were obtained by the QST2 method and were subsequently checked for the presence of imaginary frequencies. [44] Using the DFT geometries, the electronic energies of all key stationary points were calculated by a highly accurate composite DLPNO-CCSD(T)/DZ//SCS-MP2/TZ approach[45–49] (see SI for details). All DFT calculations were conducted using Gaussian 16.[50] The -SCS-MP2 and DLPNO-CCSD(T) computations were accomplished with the Orca program (ver. 5.0.0).[51,52].

In MD simulations, two different degrees of functionalisation of GCN were considered: sparse coverage (one group for each side of the graphene cell) and a system with 15 at. % (referred to as GCN-15) of coverage. Aliphatic nitriles (Fig. 2) were placed in a box of size $3 \times 3 \times 3$ nm. GCN was modelled as a periodic system with the nitrile groups positioned in the middle of a $3 \times 3 \times 10$ nm box. In this case, a flat bottom restraint of 3.2 nm from the centre of the simulation box in

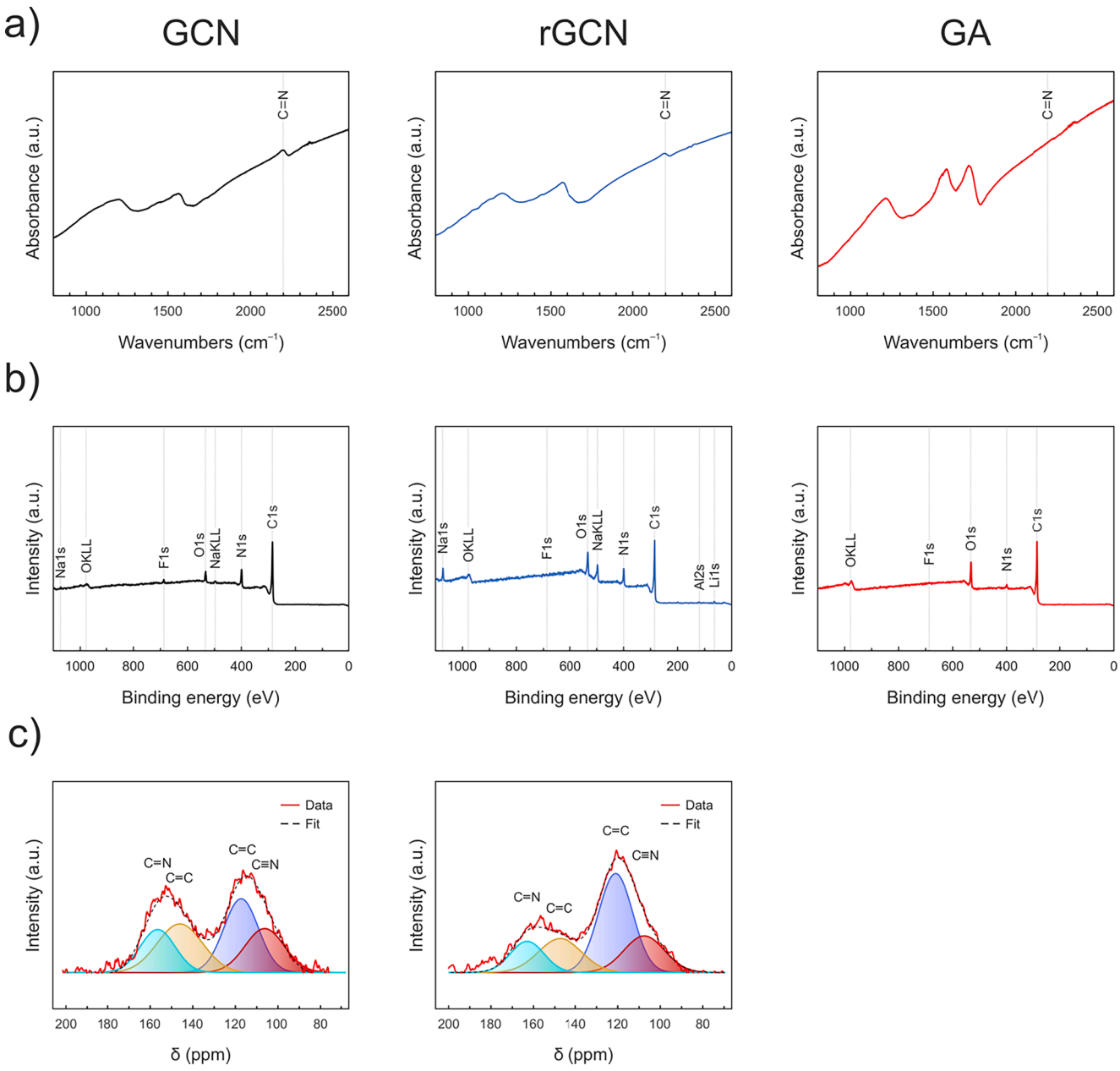

Fig. 3. a) FTIR spectra of GCN before and after the reduction reaction and GA (GCN after hydrolysis). b) XPS survey spectra for GCN, rGCN and GA. c) CP-MAS ^{13}C NMR solid-state NMR spectra of GCN and rGCN.

the z-direction was applied to prevent collisions of $LiAlH_4$ molecules. In the starting geometry, one molecule of $LiAlH_4$ for each nitrile group present in the box was added (i.e. one $LiAlH_4$ for aliphatic molecules and two $LiAlH_4$ for two-sided GCN). All systems were minimised and thermalised to a desired temperature of 300 K in the NpT ensemble prior to conducting a 300 ns production run under the NVT ensemble. The last 250 ns of this run were used for final analyses (except for the aluminium approach analysis, which was carried out using the last 100 ns). All MD simulations were carried out in the Gromacs software package.[53] Gromacs 4.5.1 was used for simulations of aliphatic molecules, whereas Gromacs 5.1.4 was used for graphene systems (flat bottom restraints were not introduced until version 5). Further details are provided in SI.

3. Results and discussion

To quantify the stability of the GCN, ^{13}C solid-state NMR spectroscopy was applied using the cross-polarization magic angle spinning (CP MAS) technique to study the behavior of GCN after treatment with $LiAlH_4$ (rGCN). The peak at 107.2 ppm was attributed to the –CN groups on GCN (Fig. 3c). After reduction, only a very slight decrease of the peak at 107.2 ppm was observed, confirming that the majority of –CN functional groups on GCN remained unaffected. This finding was also supported by FTIR spectra attained before and after the reduction reaction (Fig. 3a) showing that the peak corresponding to CN stretching (at ~2200 cm^{-1}) remains practically unchanged. Additionally, XPS shown that pure GCN and rGCN have almost identical N percentage (Fig. 3b, Table S1 and S2). Spectra of GA (i.e., hydrolyzed GN) are also included for comparison. Thus, GCN has high chemical stability under strongly reducing conditions (see SI for more experimental details).

The plausibility of the reduction of GCN by $LiAlH_4$ in THF was first explored with DFT considering solvent effects implicitly (Fig. 1b). After stabilizing the reagents in a reactant complex, formation of an imide intermediate (I-imide) was found to be kinetically feasible ($E_a = 18$ kcal/mol) and thermodynamically favourable ($\Delta_r G^\circ$ (298.15 K) = –32 kcal/

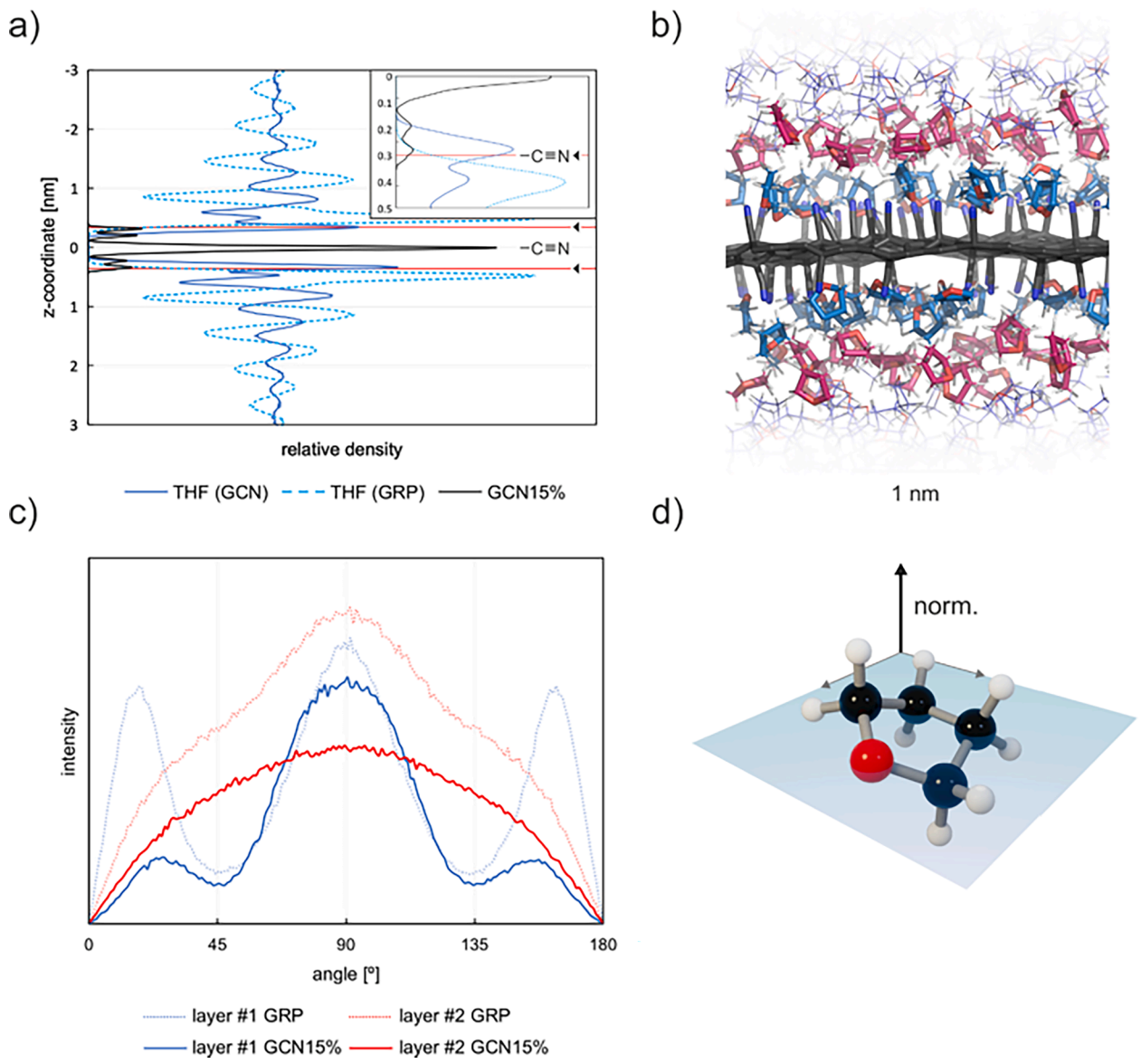

Fig. 4. a) Relative density of THF around graphene and GCN (at z = 0 nm). Inset shows a position of a –CN group within the first solvation layer. b) Representative snapshot from MD simulations showing the first (blue) and second (red) layer of THF molecules around GCN. c) Orientation of first and second layer of THF around GCN. d) The normal of the molecular plane of THF.

mol). The structure of the intermediate with both Li^+ and AlH_3 bonded to the imide nitrogen was consistent with that reported by Glaser et al. [35] for acetonitrile. Also, the energetic value of the first reduction step was found to be qualitatively similar for GCN and acetonitrile, with even larger stabilisation of the imide in the former case. The subsequent transformations to either an imine or amine were mechanistically more complex. Nevertheless, both pathways were confirmed to be thermodynamically feasible for acetonitrile. Although the formation of an imine was disfavoured in the case of GCN, its reduction to an amine was even more exergonic than that of acetonitrile ($\Delta_rG^\circ = -81.5$ kcal/mol vs. –69.5 kcal/mol). It is worth noting that the DFT data were consistent with those obtained by applying the more accurate composite DLPNO-CCSD(T)/TZ//SCS-MP2/TZ/SMD (see Table S4 for a summary of calculated energies) using the structures and frequency analysis from the DFT calculations. In summary, the activation barrier for the reduction of GCN by $LiAlH_4$ to an imide was only slightly higher and the overall process thermodynamically more favourable than the reduction of acetonitrile. However, as the reduction of acetonitrile is readily feasible, whereas GCN remains inert towards $LiAlH_4$, there must be other reasons explaining the experimentally observed resistance of GCN towards reduction.

For efficient reduction, the access and alignment of all species participating in the reaction are crucial; no reaction can occur without meeting these geometrical criteria. Hence, we focused on this mechanistic part of the reduction (processes that precede the chemical transformation described above) by means of MD simulations. To investigate possible differences between the reactivity of GCN and common organic nitriles, the accessibility of $LiAlH_4$ to nitrile groups grafted on graphene was compared with that towards a series of aliphatic nitriles with different carbon chain lengths (Fig. 2) in THF, which is a versatile solvent commonly used for this type of reduction reaction.

First, the arrangement of solvent molecules induced by the surface of pristine (unfunctionalised) graphene (GRP) was studied. It was shown that similarly to water (and many other solvents),[54] THF molecules formed several distinct layers close to graphene (Fig. 4a). Moreover, the structuring of THF was evident in the case of GCN-15, i.e. a surface bearing 15 % of nitrile groups which induced a similar layered solvent arrangement. This more compact organisation largely resulted from the

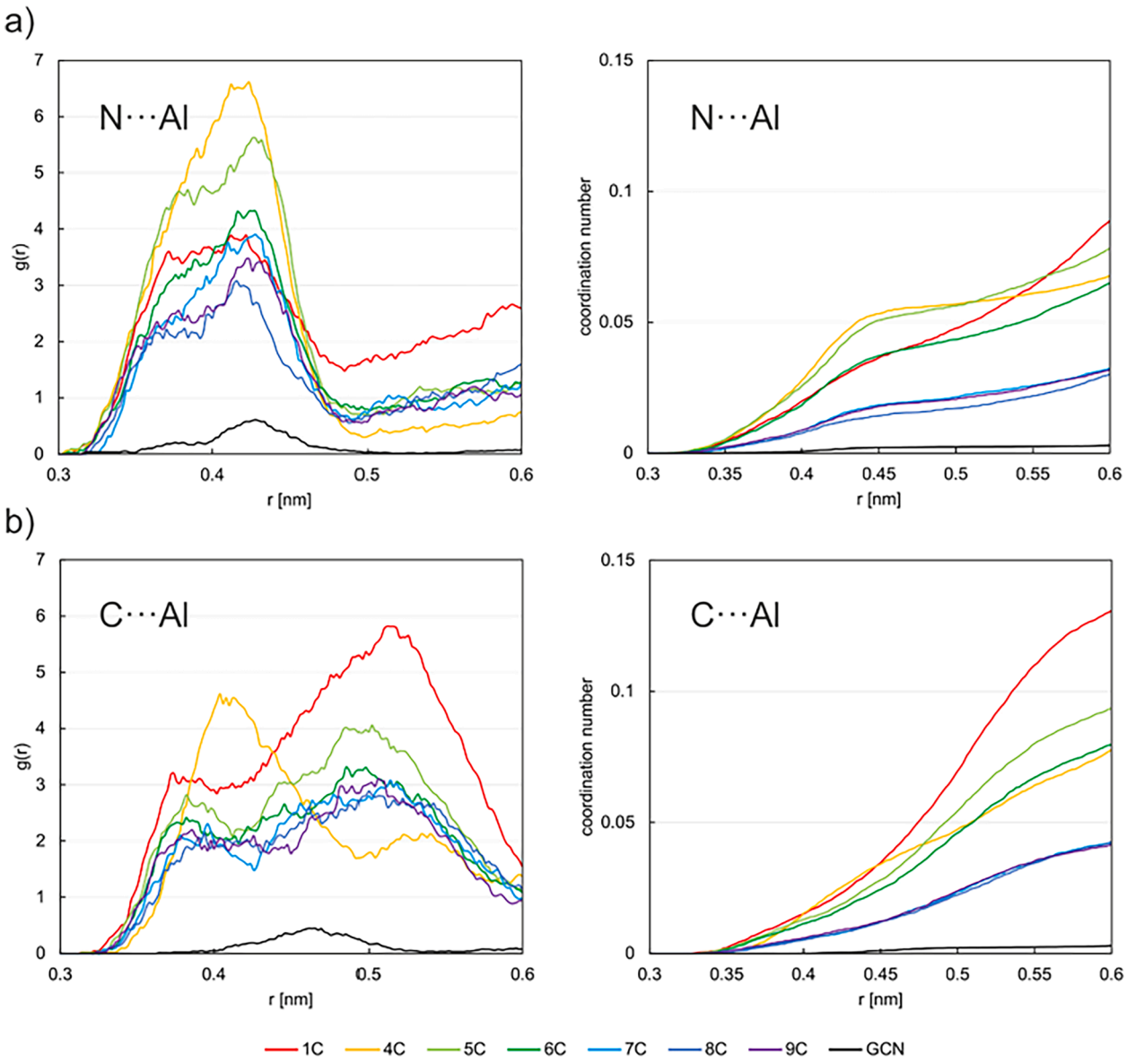

Fig. 5. Radial distribution function g(r) and corresponding coordination number between Al and a) N or b) C of the nitrile group of the studied aliphatic structures and GCN.

greater rigidity of the densely functionalised system. 78 % of THF molecules within the first solvation layer were arranged perpendicular to graphene, forming a compact and dense 0.36 nm wide layer of THF molecules (Fig. 4b). To quantify the orientation of THF molecules in the first two solvation layers, angles defined by the normal of the molecular plane with respect to the surface were measured. All molecules up to 0.6 nm from the surface were considered as the first layer, whereas the second layer constituted molecules in the range 0.6–1.05 nm from graphene. Structuring of THF molecules in the first solvation layer resulted in its high density (blue line in Fig. 4c), whereas the orientation of THF molecules in the second solvation layer was less spatially confined, without significant preference for the THF orientation pattern (red line in Fig. 4c). The –CN groups were localised within the first solvation layer (or entirely beneath the layer in the case of sparsely functionalised GCN) (cf. inset of Fig. 4a), which might suggest that access to the –CN group by $LiAlH_4$ was significantly hampered by the presence of such condensed and structured layers of the solvent molecules owing to sterical hindrance.[55].

In the next step, the accessibility of individual reactive components (Li^+ and AlH_4^-, $c \approx 0.05$ M) to the nitrile moiety to form a pre-reaction state was inspected. The residence times of the AlH_4^- ion in the vicinity (closer than 0.5 nm) of the –CN group in the aliphatic nitriles (cf. Fig. 2) did not significantly depend on the carbon-chain length and were similar to those observed for GCN, reaching 0.26 ns (Table S3, Figure S1). In simulations, Li^+ ions closely accompanied the hydride anions, and thus their residence times were analogous. The nitrile group accessibility was further analysed in terms of radial distribution functions (RDFs) of aluminium with respect to the N or C atoms of the nitrile group and the corresponding coordination numbers (Fig. 5), which are simple metrics for comparison of individual systems. Generally, increasing the alkyl chain length in the aliphatic nitrile structure led to a decrease in the coordination number of the nitrile carbon, which was even more pronounced for long molecules with an even number of carbons in the structure (Fig. 5b). This effect was due to free rotation of the carbon chain around single bonds, resulting in a larger excluded volume (Fig. 7) and thus larger steric hindrance of the hydride anion from the CN group. [56] In the case of the shortest nitrile, i.e. acetonitrile (Fig. 2; 1C), no substantial hindrance was expected. Thus, access of the reducing agent to the nitrile moiety was considered unrestricted. In accordance, the coordination number to the nitrile carbon in acetonitrile reached a

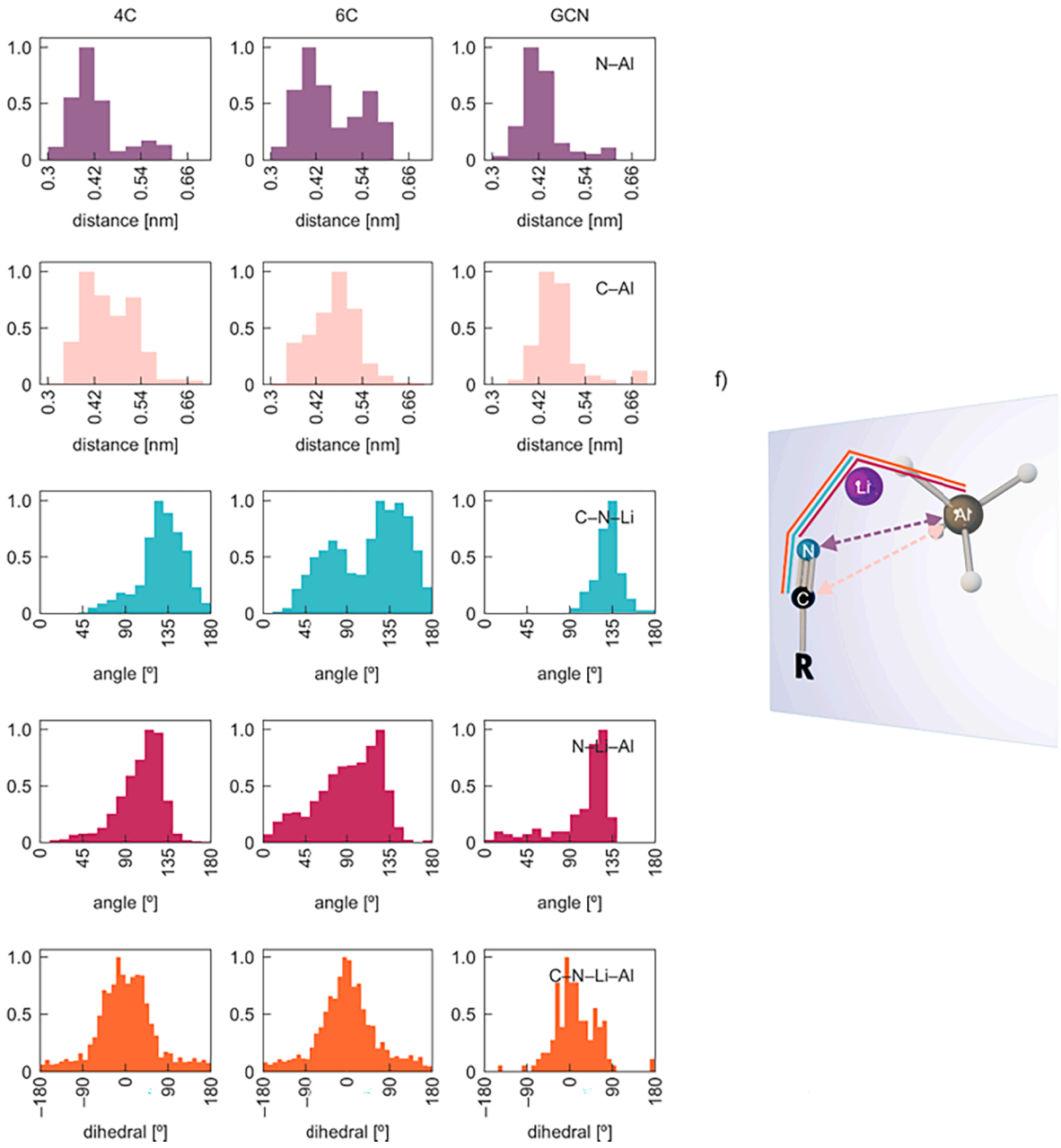

Fig. 6. Histograms showing the distances between a) nitrogen (purple) and b) carbon (pink) of the CN group and aluminium, c) angle C-N-Li (green), d) angle N-Li-Al (red), and e) dihedral angle C-N-Li-Al (orange). Only samples with the distance between Al and CN closer than 0.5 nm were considered. f) $LiAlH_4$ alignment with the nitrile group in one plane with highlighted distances (dashed lines) and angles (solid lines).

maximum value among the studied systems. On the other hand, if the methyl group was replaced by a bulkier tertiary butyl moiety (Fig. 2; 4C), the accessibility of the nitrile carbon decreased considerably and was further reduced in long carbon-chain nitriles. This trend could also be observed in the accessibility of the N atom (except for acetonitrile) but less strikingly because the nitrile group projected into the environment without any significant hindrance. The different trends of acetonitrile (Fig. 5, red curves) indicated that the access mechanism of AlH_4^- to the nitrile group differed from the other studied molecules (see below). The most dramatic decrease in accessibility of the CN group was observed in the case of sparsely functionalised GCN, which was reflected in the lowest coordination numbers (Fig. 5). Similarly, GCN-15 with a functionalisation degree of 15 % exhibited limited accessibility for the initial reduction step comparable to that of long aliphatic nitriles (Figure S2). However, due to the heterogeneous nature of the GCN-15 surface, the reduction would be a more complex process, making direct comparison with the mono-substituted systems difficult.

The final accessibility could thus be attributed to a combination of several factors: i) THF organisation at the surface, ii) immersion of the –CN group within/beneath the solvation structure, and iii) effect of the surface on the number of possible effective collisions of the reducing species with –CN. Solvent organisation close to the graphene layer (as discussed above) created a barrier for access of the AlH_4^- to the reduction centre. Thus, the anion was not able to enter even the first solvent layer (the mean distance of the aluminium atom from the graphene plane was 0.82 ± 0.1 nm) and the –CN group remained beneath the dense solvent layer. This resulted in very limited accessibility to the reactive carbon centre of GCN. Similarly, the graphene plane and its restricted space decreased dramatically the number of possible effective collisions between the reducing agent and the –CN group.

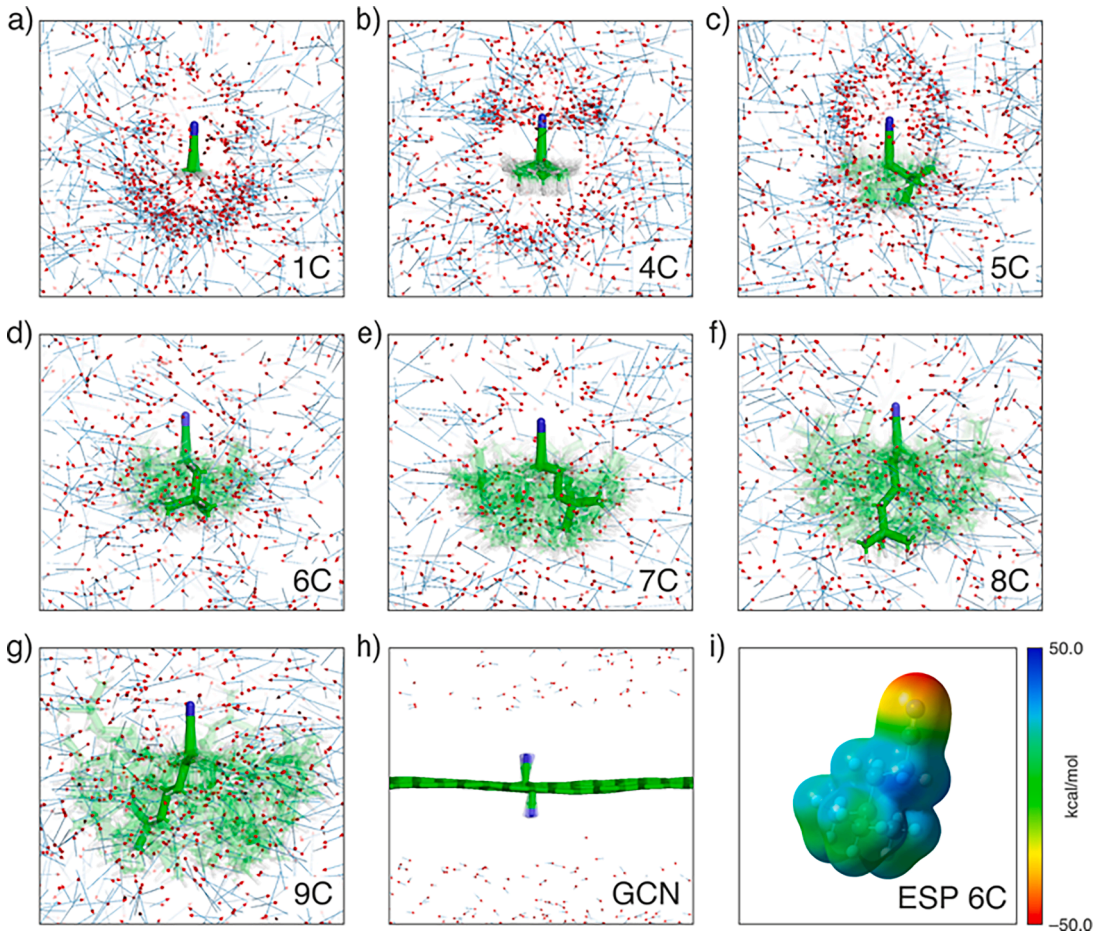

Fig. 7. a-h) CN group accessibility by a hydride anion (denoted by arrows with specified direction in red) calculated for different nitriles (the structure movement is shown by transparent shading). i) Electrostatic potential of the 6C structure showing a positive potential around the alpha carbon from the CN group (calculated at the HF/6-31G(d) level; bottom right panel).

Equally important for successful reduction is the mutual alignment of the nitrile group and $LiAlH_4$. The reaction centre in the nitrile reduction reaction must be close enough and properly aligned for an effective reduction process. Therefore, to better identify the exact mutual orientation, the angles between C-N-Li and N-Li-Al atoms, and the torsion angle C-N-Li-Al were calculated (Figs. 6 and S3).

Two aliphatic nitriles (4C and 6C, Fig. 2) differing in length and GCN were selected for such analysis. The corresponding histograms showed that in the case of 6C, two distinct arrangements (two bands in panels 5a and 5c) were observed with strong in-plane alignment (narrow dihedral angle distribution). In the case of a shorter 4C chain, only one dominant orientation without proper alignment (a notably wider dihedral angle distribution ranging from –50° to 50°) was found. The branched *tert*-butyl structure did not allow easy access of the reducing agent from the methyl side of the CN group. This behaviour was even more pronounced in sparse GCN (which was reflected in much narrower distributions), with the accessibility restricted by the graphene layer on one side and by highly ordered solvent molecules on the other. In contrast, 6C displayed the least steric hindrance between $LiAlH_4$ and the functional group, and thus the reducing agent could easily access the reaction site.

Finally, a detailed analysis of the accessibility of AlH_4^- to the reduction centre showed qualitative differences among the studied systems (Fig. 7a-h). Generally, short-chain structures (1C, 4C and 5C, Fig. 2) and the corresponding AlH_4^- approaching mechanisms differed significantly from other structures. The shortest-chain nitrile, acetonitrile (1C), preferred access of AlH_4^- from its far side (i.e. methyl side). With increasing steric hindrance of the CN group in longer chain nitriles (4C and 5C), this mechanism became more difficult and attack from the near side became preferable. For example, in 4C (Fig. 7b), the bulky *tert*-butyl group served as an effective steric barrier, which resulted in a complete change in the preferential access of AlH_4^-, with a sharp transition between near-side and far-side access modes. Similarly, the structure with 5C favoured near-side attack (Fig. 7c), although the boundary was not as sharp as for 4C. In the case of longer chains (6C, 7C, 8C and 9C, Fig. 2), the hydride anion approached predominantly from the aliphatic side of molecules. This can be rationalised in terms of the electrostatic potential (ESP) generated by the molecule, where the positive potential around the exposed α-carbon of the CN group may attract AlH_4^- (Fig. 7i), and thus determine the accessibility. However, the final accessibility will be a combination of two independent contributions: i) electrostatic attraction, and ii) steric hindrance as the aliphatic carbon chain is increased. In addition, long chains with an even number of carbon atoms (here, 8C) showed a larger excluded volume than odd number carbon structures, decreasing the resulting group accessibility. In the case of sparsely distributed GCN, only a very low number of aluminium hydride species were located near the surface, which hardly passed through the solvent layer. Thus, the graphene network served as an efficient steric hindering group protecting nitrile groups from reduction by $LiAlH_4$.

4. Conclusions

In the present work, we demonstrated differences in the mechanistic aspects of reduction reactions of aliphatic nitriles and GCN with $LiAlH_4$. Since the reaction thermodynamics and kinetics alone could not explain the resistance of GCN towards reduction, we performed a series of MD simulations to investigate the mechanical and steric contributions of the

graphene surface to the –CN reduction reaction. Theoretical simulations of aliphatic nitriles in a THF medium showed substantial differences in molecular accessibility of AlH_4^- to the reaction centre based on the different molecular topology and length of the aliphatic chains. Moreover, the main access direction of attacking AlH_4^- anions varied considerably with the size of the studied structures. The overall accessibility was governed by a combination of two independent factors, electrostatic attraction and steric hindrance of the aliphatic carbon chain. In GCN, the surface induced strong layering of THF molecules on one side and the graphene network on the other side resulted in an ultimate access barrier, and thus poor accessibility of the grafted –CN group. The space constraint of the 2D framework may act as a versatile protective group in a variety of organic reactions. We showed that interfacial phenomena play important role in the reactivity of graphene derivatives.

CRediT authorship contribution statement

Martin Pykal: Conceptualization, Investigation, Writing – original draft, Visualization. **Martin Vondrák:** Investigation, Writing – original draft. **Martin Šrejber:** Writing – review & editing. **Iosif Tantis:** Investigation. **Elmira Mohammadi:** Investigation. **Aristides Bakandritsos:** Writing – review & editing. **Miroslav Medveď:** Investigation, Writing – review & editing. **Michal Otyepka:** Conceptualization, Writing – review & editing, Supervision.

Declaration of Competing Interest

The authors declare that they have no known competing financial interests or personal relationships that could have appeared to influence the work reported in this paper.

Acknowledgement

The authors acknowledge support from the ERDF/ESF project “Nano4Future” (No. CZ.02.1.01/0.0/0.0/16_019/0000754) of the Ministry of Education, Youth and Sports of the Czech Republic. MO acknowledges support by ERC project No. 683024 from the European Union’s Horizon 2020.

Appendix A. Supplementary data

Supplementary data to this article can be found online at https://doi.org/10.1016/j.apsusc.2022.153792.

References

[1] A.K. Geim, K.S. Novoselov, The rise of graphene, Nat. Mater. 6 (2007) 183–191, https://doi.org/10.1038/nmat1849.
[2] K.S. Novoselov, V.I. Fal’ko, L. Colombo, P.R. Gellert, M.G. Schwab, K. Kim, A roadmap for graphene, Nature 490 (2012) 192–200, https://doi.org/10.1038/nature11458.
[3] E. Vermisoglou, D. Panáček, K. Jayaramulu, M. Pykal, I. Frébort, M. Kolář, M. Hajdúch, R. Zbořil, M. Otyepka, Human virus detection with graphene-based materials, Biosens. Bioelectron. 166 (2020), 112436, https://doi.org/10.1016/j.bios.2020.112436.
[4] S.K. Min, W.Y. Kim, Y. Cho, K.S. Kim, Fast DNA sequencing with a graphene-based nanochannel device, Nat. Nanotechnol. 6 (2011) 162–165, https://doi.org/10.1038/nnano.2010.283.
[5] R. Raccichini, A. Varzi, S. Passerini, B. Scrosati, The role of graphene for electrochemical energy storage, Nat. Mater. 14 (2014) 271–279, https://doi.org/10.1038/nmat4170.
[6] Y. Han, Z. Xu, C. Gao, Ultrathin Graphene Nanofiltration Membrane for Water Purification, Adv. Funct. Mater. 23 (2013) 3693–3700, https://doi.org/10.1002/adfm.201202601.
[7] J. Zhao, W. Ren, H.-M. Cheng, Graphene sponge for efficient and repeatable adsorption and desorption of water contaminations, J. Mater. Chem. 22 (2012) 20197, https://doi.org/10.1039/c2jm34128j.
[8] K. Yang, L. Feng, X. Shi, Z. Liu, Nano-graphene in biomedicine: theranostic applications, Chem. Soc. Rev. 42 (2013) 530–547, https://doi.org/10.1039/C2CS35342C.
[9] J. Liu, L. Cui, D. Losic, Graphene and graphene oxide as new nanocarriers for drug delivery applications, Acta Biomater. 9 (2013) 9243–9257, https://doi.org/10.1016/j.actbio.2013.08.016.
[10] J. Wu, L. Jia, Y. Zhang, Y. Qu, B. Jia, D.J. Moss, Graphene Oxide for Integrated Photonics and Flat Optics, Adv. Mater. 3 (2021), 2006415, https://doi.org/10.1002/adma.202006415.
[11] M. Long, P. Wang, H. Fang, W. Hu, Progress, challenges, and opportunities for 2D material based photodetectors, Adv. Funct. Mater. 29 (2019) 1803807, https://doi.org/10.1002/adfm.201803807.
[12] S. Stankovich, D.A. Dikin, G.H.B. Dommett, K.M. Kohlhaas, E.J. Zimney, E. A. Stach, R.D. Piner, S.T. Nguyen, R.S. Ruoff, Graphene-based composite materials, Nature 442 (2006) 282–286, https://doi.org/10.1038/nature04969.
[13] V.B. Mohan, K. Lau, D. Hui, D. Bhattacharyya, Graphene-based materials and their composites: A review on production, applications and product limitations, Compos. Part B Eng. 142 (2018) 200–220, https://doi.org/10.1016/j.compositesb.2018.01.013.
[14] L. Liao, D. Peng, Z. Liu, Chemistry makes graphene beyond graphene, J. Am. Chem. Soc. 136 (2014) 12194–12200, https://doi.org/10.1021/ja5048297.
[15] C. Wang, K. Xia, H. Wang, X. Liang, Z. Yin, Y. Zhang, Advanced carbon for flexible and wearable electronics, Adv. Mater. 31 (2019) 1801072, https://doi.org/10.1002/adma.201801072.
[16] M.C. Vu, N.A. Thi Thieu, J.-H. Lim, W.-K. Choi, J. Chan Won, M.A. Islam, S.-R. Kim, Ultrathin thermally conductive yet electrically insulating exfoliated graphene fluoride film for high performance heat dissipation, Carbon. 157 (2020) 741–749, https://doi.org/10.1016/j.carbon.2019.10.079.
[17] F. Karlický, R. Zbořil, M. Otyepka, Band gaps and structural properties of graphene halides and their derivates: A hybrid functional study with localized orbital basis sets, J. Chem. Phys. 137 (3) (2012) 034709, https://doi.org/10.1063/1.4736998.
[18] J. Tuček, P. Błoński, J. Ugolotti, A.K. Swain, T. Enoki, R. Zbořil, Emerging chemical strategies for imprinting magnetism in graphene and related 2D materials for spintronic and biomedical applications, Chem. Soc. Rev. 47 (2018) 3899–3990, https://doi.org/10.1039/C7CS00288B.
[19] Y.J. Shin, Y. Wang, H. Huang, G. Kalon, A.T.S. Wee, Z. Shen, C.S. Bhatia, H. Yang, Surface-energy engineering of graphene, Langmuir. 26 (2010) 3798–3802, https://doi.org/10.1021/la100231u.
[20] A. Eftekhari, H. Garcia, The necessity of structural irregularities for the chemical applications of graphene, Mater. Today Chem. 4 (2017) 1–16, https://doi.org/10.1016/j.mtchem.2017.02.003.
[21] M.A. Bissett, S. Konabe, S. Okada, M. Tsuji, H. Ago, Enhanced chemical reactivity of graphene induced by mechanical strain, ACS Nano. 7 (2013) 10335–10343, https://doi.org/10.1021/nn404746h.
[22] D. Chen, H. Feng, J. Li, Graphene oxide: Preparation, functionalization, and electrochemical applications, Chem. Rev. 112 (2012) 6027–6053, https://doi.org/10.1021/cr300115g.
[23] C.K. Chua, Z. Sofer, M. Pumera, Graphite oxides: Effects of permanganate and chlorate oxidants on the oxygen composition, Chem. Eur. J. 18 (2012) 13453–13459, https://doi.org/10.1002/chem.201202320.
[24] D.D. Chronopoulos, A. Bakandritsos, M. Pykal, R. Zbořil, M. Otyepka, Chemistry, properties, and applications of fluorographene, Appl. Mater. Today. 9 (2017) 60–70, https://doi.org/10.1016/j.apmt.2017.05.004.
[25] J. Sturala, J. Luxa, M. Pumera, Z. Sofer, Chemistry of graphene derivatives: Synthesis, applications, and perspectives, Chem. Eur. J. 24 (2018) 5992–6006, https://doi.org/10.1002/chem.201704192.
[26] M. Dubecký, E. Otyepková, P. Lazar, F. Karlický, M. Petr, K. Čépe, P. Banáš, R. Zbořil, M. Otyepka, Reactivity of Fluorographene: A Facile Way toward Graphene Derivatives, J. Phys. Chem. Lett. 6 (2015) 1430–1434, https://doi.org/10.1021/acs.jpclett.5b00565.
[27] M. Medveď, G. Zoppellaro, J. Ugolotti, D. Matochová, P. Lazar, T. Pospíšil, A. Bakandritsos, J. Tuček, R. Zbořil, M. Otyepka, Reactivity of fluorographene is triggered by point defects: beyond the perfect 2D world, Nanoscale. 10 (2018) 4696–4707, https://doi.org/10.1039/C7NR09426D.
[28] A. Bakandritsos, M. Pykal, P. Błoński, P. Jakubec, D.D. Chronopoulos, K. Poláková, V. Georgakilas, K. Čépe, O. Tomanec, V. Ranc, A.B. Bourlinos, R. Zbořil, M. Otyepka, Cyanographene and graphene acid: Emerging derivatives enabling high-yield and selective functionalization of graphene, ACS Nano. 11 (2017) 2982–2991, https://doi.org/10.1021/acsnano.6b08449.
[29] V. Aureggi, G. Sedelmeier, 1,3-Dipolar cycloaddition: Click chemistry for the synthesis of 5-substituted tetrazoles from organoaluminum azides and nitriles, Angew. Chemie Int. Ed. 46 (2007) 8440–8444, https://doi.org/10.1002/anie.200701045.
[30] L. Bosch, J. Vilarrasa, $C_2(OTf)_2$-catalyzed and microwave-controlled preparation of tetrazoles from nitriles and organic azides under mild, safe conditions, Angew. Chemie Int. Ed. 46 (2007) 3926–3930, https://doi.org/10.1002/anie.200605095.
[31] N. Nishiwaki, K. Kobiro, S. Hirao, J. Sawayama, K. Saigo, Y. Ise, Y. Okajima, M. Ariga, Inverse electron-demand 1,3-dipolar cycloaddition of nitrile oxide with common nitriles leading to 3-functionalized 1,2,4-oxadiazoles, Org. Biomol. Chem. 9 (2011) 6750, https://doi.org/10.1039/c1ob05682d.
[32] B. Heller, B. Sundermann, H. Buschmann, H.-J. Drexler, J. You, U. Holzgrabe, E. Heller, G. Oehme, Photocatalyzed [2 + 2 + 2]-cycloaddition of nitriles with acetylene: An effective method for the synthesis of 2-pyridines under mild conditions, J. Org. Chem. 67 (2002) 4414–4422, https://doi.org/10.1021/jo011032n.
[33] D. Enders, J.P. Shilvock, Some recent applications of α-amino nitrile chemistry, Chem. Soc. Rev. 29 (2000) 359–373, https://doi.org/10.1039/a908290e.

[34] R. Bruckner. Organic Mechanisms: Reactions, Stereochemistry and Synthesis, 1 ed., Springer-Verlag Berlin Heidelberg, Berlin, Heidelberg, 2010 https://doi.org/10.1007/978-3-642-03651-4.
[35] R. Glaser, L. Ulmer, S. Coyle, Mechanistic models for LAH reductions of acetonitrile and malononitrile. Aggregation effects of Li^+ and AlH_3 on imide–enamide equilibria, J. Org. Chem. 78 (2013) 1113–1126, https://doi.org/10.1021/jo302527k.
[36] Y. Hori, T. Ida, M. Mizuno, A comparative theoretical study of the hydride transfer mechanisms during $LiAlH_4$ and $LiBH_4$ reductions, Comput. Theor. Chem. 1076 (2016) 86–93, https://doi.org/10.1016/j.comptc.2015.12.014.
[37] A. Ambrosi, C.K. Chua, A. Bonanni, M. Pumera, Lithium aluminum hydride as reducing agent for chemically reduced graphene oxides, Chem. Mater. 24 (2012) 2292–2298, https://doi.org/10.1021/cm300382b.
[38] S. Eigler, Y. Hu, Y. Ishii, A. Hirsch, Controlled functionalization of graphene oxide with sodium azide, Nanoscale 5 (2013), 12136, https://doi.org/10.1039/c3nr04332k.
[39] D. Bouša, V. Mazánek, D. Sedmidubský, O. Jankovský, M. Pumera, Z. Sofer, Hydrogenation of fluorographite and fluorographene: An easy way to produce highly hydrogenated graphene, Chem. Eur. J. 24 (2018) 8350–8360, https://doi.org/10.1002/chem.201800236.
[40] R. Salvio, S. Krabbenborg, W.J.M. Naber, A.H. Velders, D.N. Reinhoudt, W.G. van der Wiel, The formation of large-area conducting graphene-like platelets, Chem. Eur. J. 15 (2009) 8235–8240, https://doi.org/10.1002/chem.200900661.
[41] J.-D. Chai, M. Head-Gordon, Long-range corrected hybrid density functionals with damped atom–atom dispersion corrections, Phys. Chem. Chem. Phys. 10 (2008) 6615, https://doi.org/10.1039/b810189b.
[42] T.H. Dunning, Gaussian basis sets for use in correlated molecular calculations. I. The atoms boron through neon and hydrogen, J. Chem. Phys. 90 (2) (1989) 1007–1023, https://doi.org/10.1063/1.456153.
[43] A.V. Marenich, C.J. Cramer, D.G. Truhlar, Universal solvation model based on solute electron density and on a continuum model of the solvent defined by the bulk dielectric constant and atomic surface tensions, J. Phys. Chem. B. 113 (2009) 6378–6396, https://doi.org/10.1021/jp810292n.
[44] C. Peng, H. Bernhard Schlegel, Combining synchronous transit and quasi-Newton methods to find transition states, Isr. J. Chem. 33 (1993) 449–454, https://doi.org/10.1002/ijch.199300051.
[45] S. Grimme, Improved second-order Møller-Plesset perturbation theory by separate scaling of parallel- and antiparallel-spin pair correlation energies, J. Chem. Phys. 118 (2003) 9095–9102, https://doi.org/10.1063/1.1569242.
[46] M. Feyereisen, G. Fitzgerald, A. Komornicki, Use of approximate integrals in ab initio theory. An application in MP2 energy calculations, Chem. Phys. Lett. 208 (5–6) (1993) 359–363, https://doi.org/10.1016/0009-2614(93)87156-W.
[47] C. Riplinger, P. Pinski, U. Becker, E.F. Valeev, F. Neese, Sparse maps—A systematic infrastructure for reduced-scaling electronic structure methods. II. Linear scaling domain based pair natural orbital coupled cluster theory, J. Chem. Phys. 144 (2) (2016) 024109, https://doi.org/10.1063/1.4939030.
[48] G.D. Purvis, R.J. Bartlett, A full coupled-cluster singles and doubles model: The inclusion of disconnected triples, J. Chem. Phys. 76 (1982) 1910–1918, https://doi.org/10.1063/1.443164.
[49] D.G. Liakos, M. Sparta, M.K. Kesharwani, J.M.L. Martin, F. Neese, Exploring the accuracy limits of local pair natural orbital coupled-cluster theory, J. Chem. Theory Comput. 11 (2015) 1525–1539, https://doi.org/10.1021/ct501129s.
[50] M.J. Frisch, G.W. Trucks, H.B. Schlegel, G.E. Scuseria, M.A. Robb, J.R. Cheeseman, G. Scalmani, V. Barone, G.A. Petersson, H. Nakatsuji, X. Li, M. Caricato, A. V. Marenich, J. Bloino, B.G. Janesko, R. Gomperts, B. Mennucci, H.P. Hratchian, J. V. Ortiz, A.F. Izmaylov, J.L. Sonnenberg, D. Williams-Young, F. Ding, F. Lipparini, F. Egidi, J. Goings, B. Peng, A. Petrone, T. Henderson, D. Ranasinghe, V. G. Zakrzewski, J. Gao, N. Rega, G. Zheng, W. Liang, M. Hada, M. Ehara, K. Toyota, R. Fukuda, J. Hasegawa, M. Ishida, T. Nakajima, Y. Honda, O. Kitao, H. Nakai, T. Vreven, K. Throssell, J.A. Montgomery Jr., J.E. Peralta, F. Ogliaro, M. J. Bearpark, J.J. Heyd, E.N. Brothers, K.N. Kudin, V.N. Staroverov, T.A. Keith, R. Kobayashi, J. Normand, K. Raghavachari, A.P. Rendell, J.C. Burant, S.S. Iyengar, J. Tomasi, M. Cossi, J.M. Millam, M. Klene, C. Adamo, R. Cammi, J.W. Ochterski, R.L. Martin, K. Morokuma, O. Farkas, J.B. Foresman, D.J. Fox, Gaussian 16 Revision B.01 (2016).
[51] F. Neese, The ORCA program system, WIREs Comput. Mol. Sci. 2 (2012) 73–78, https://doi.org/10.1002/wcms.81.
[52] F. Neese, Software update: the ORCA program system, version 4.0, WIREs Comput, Mol. Sci. 8 (2018), e1327, https://doi.org/10.1002/wcms.1327.
[53] D. Van Der Spoel, E. Lindahl, B. Hess, G. Groenhof, A.E. Mark, H.J.C. Berendsen, GROMACS: Fast, flexible, and free, J. Comput. Chem. 26 (2005) 1701–1718, https://doi.org/10.1002/jcc.20291.
[54] F. Goujon, A. Ghoufi, P. Malfreyt, Associated molecular liquids at the graphene monolayer interface, J. Chem. Phys. 154 (10) (2021) 104504, https://doi.org/10.1063/5.0042438.
[55] C.-J. Shih, S. Lin, M.S. Strano, D. Blankschtein, Understanding the stabilization of liquid-phase-exfoliated graphene in polar solvents: Molecular dynamics simulations and kinetic theory of colloid aggregation, J. Am. Chem. Soc. 132 (2010) 14638–14648, https://doi.org/10.1021/ja1064284.
[56] D. Konatham, A. Striolo, Molecular design of stable graphene nanosheets dispersions, Nano Lett. 8 (2008) 4630–4641, https://doi.org/10.1021/nl802262p.
[57] A.S. Dobrota, I.A. Pašti, S.V. Mentus, B. Johansson, N.V. Skorodumova, Altering the reactivity of pristine, N- and P-doped graphene by strain engineering: A DFT view on energy related aspects, Appl. Surf. Sci. 514 (2020) 145937, https://doi.org/10.1016/j.apsusc.2020.145937.